First operation of a Free-Electron Laser generating GW power radiation at 32 nm wavelength

V. Ayvazyan[6], N. Baboi[6], J. Bähr[7], V. Balandin[6], B. Beutner[9], A. Brandt[6], I. Bohnet[6], A. Bolzmann[2], R. Brinkmann[6], O.I. Brovko[15], J.P. Carneiro[6], S. Casalbuoni[6], M. Castellano[11], P. Castro[6], L. Catani[13], E. Chiadroni[13], S. Choroba[6], A. Cianchi[13], H. Delsim-Hashemi[9], G. Di Pirro[11], M. Dohlus[6], S. Düsterer[6], H.T. Edwards[8], B. Faatz[6], A.A. Fateev[15], J. Feldhaus[6], K. Flöttmann[6], J. Frisch[18], L. Fröhlich[9], T. Garvey[16], U. Gensch[7], N. Golubeva[6], H.-J. Grabosch[7], B. Grigoryan[4], O. Grimm[6], U. Hahn[6], J.H. Han[7], M. v. Hartrott[3], K. Honkavaara[9], M. Hüning[6], R. Ischebeck[6], E. Jaeschke[3], M. Jablonka[1], R. Kammering[6], V. Katalev[6], B. Keitel[6,*] S. Khodyachykh[7], Y. Kim[6], V. Kocharyan[6], M. Körfer[6], M. Kollewe[6], D. Kostin[6], D. Krämer[3], M. Krassilnikov[7], G. Kube[6], L. Lilje[6], T. Limberg[6], D. Lipka[3], F. Löhl[9], M. Luong[1], C. Magne[1], J. Menzel[6], P. Michelato[12], V. Miltchev[7], M. Minty[6], W.D. Möller[6], L. Monaco[12], W. Müller[5], M. Nagl[6], O. Napoly[1], P. Nicolosi[10], D. Nölle[6], T. Nuñez[6], A. Oppelt[7], C. Pagani[12], R. Paparella[1], B. Petersen[6], B. Petrosyan[7], J. Pflüger[6], P. Piot[8], E. Plönjes[6], L. Poletto[10], D. Proch[6], D. Pugachov[6], K. Rehlich[6], D. Richter[3], S. Riemann[7], M. Ross[18], J. Rossbach[9,†], M. Sachwitz[7], E.L.Saldin[6], W. Sandner[17], H. Schlarb[6], B. Schmidt[6], M. Schmitz[6], P. Schmüser[9], J.R. Schneider[6], E.A. Schneidmiller[6], H.-J. Schreiber[7], S. Schreiber[6], A.V. Shabunov[15], D. Sertore[12], S. Setzer[5], S. Simrock[6], E. Sombrowski[6], L. Staykov[7], B. Steffen[6], F. Stephan[7], F. Stulle[6], K.P. Sytchev[15], H. Thom[6], K. Tiedtke[6], M. Tischer[6], R. Treusch[6], D. Trines[6], I. Tsakov[14], A. Vardanyan[4], R. Wanzenberg[6], T. Weiland[5], H. Weise[6], M. Wendt[6], I. Will[17], A. Winter[6], K. Wittenburg[6], M.V. Yurkov[6], I. Zagorodnov[5], P. Zambolin[10], K. Zapfe[6]

[*] Present address: Infineon Technologies, Dresden

[†] Corresponding author

[1]CEA Saclay, 91191 Gif-sur-Yvette, France

[2]Bayerische Julius-Maximilians Universität, Inst. f. Theor. Physik u. Astrophysik, Am Hubland, 97074 Würzburg, Germany

[3]BESSY GmbH, Albert-Einstein-Str.15, 12489 Berlin, Germany

[4]Center for the Advancement of Natural Discoveries using Light Emission CANDLE, Acharyan 31, 375040 Yerevan, Armenia

[5]Technische Universität Darmstadt, FB 18, Institut TEMF, Schlossgartenstr. 8, 64289 Darmstadt, Germany

[6]Deutsches Elektronen-Synchrotron DESY, Notkestrasse 85, 22603 Hamburg, Germany

[7]Deutsches Elektronen-Synchrotron DESY, Platanenallee 6, 15738 Zeuthen, Germany

[8]Fermi National Accelerator Laboratory, MS 306, P.O.Box 500, Batavia, IL 60510 USA

[9]Universität Hamburg, Inst. f. Experimentalphysik, Luruper Chaussee 149, 22761 Hamburg, Germany

[10]INFM, Dept. of Information Engineering, University of Padova, via Gradenigo 6/A, 35131 Padova, Italy

[11]INFN-LNF, via E. Fermi 40, 00044 Frascati, Italy

[12]INFN Milano-LASA, via Fratelli Cervi 201,l 20090 Segrate (MI), Italy

[13]INFN-Roma2, via della Ricerca Scientifica 1, 00100 Roma, Italy

[14]Institute for Nuclear Researches and Nuclear Energy, Tzarigradsko Shaussee Boulevard 72, 1784 Sofia, Bulgaria

[15]Joint Institute for Nuclear Research, 141980 Dubna, Moscow Region, Russia

[16]Laboratoire de L'Accélérateur Linéaire, IN2P3-CNRS, Université de Paris-Sud, B.P. 34, 91898 Orsay, France

[17] Max-Born-Institute, Max-Born-Str. 2a, 12489 Berlin, Germany

[18]Stanford Linear Accelerator Center, 2575 Sand Hill Road, Menlo Park, CA 94025, USA

ABSTRACT

Many scientific disciplines ranging from physics, chemistry and biology to material sciences, geophysics and medical diagnostics need a powerful X-ray source with pulse lengths in the femtosecond range[1-4]. This would allow, for example, time-resolved observation of chemical reactions with atomic resolution. Such radiation of extreme intensity, and tunable over a wide range of wavelengths, can be accomplished using high-gain free-electron lasers (FEL)[5-10]. Here we present results of the first successful operation of an FEL at a wavelength of 32 nm, with ultra-short pulses (25 fs FWHM), a peak power at the Gigawatt level, and a high degree of transverse and longitudinal coherence. The experimental data are in full agreement with theory. This is the shortest wavelength achieved with an FEL to date and an important milestone towards a user facility designed for wavelengths down to 6 nm. With a peak brilliance exceeding the state-of-the-art of synchrotron radiation sources[4] by seven orders of magnitude, this device opens a new field of experiments, and it paves the way towards sources with even shorter wavelengths, such as the Linac Coherent Light Source[3] at Stanford, USA, and the European X-ray Free Electron Laser Facility[4] in Hamburg, Germany.

PACS numbers: 41.60.Cr,29.17.+w,29.27.-a.Fh,41.75.Lx,29.25.Bx,52.75.Va

1 Introduction

The main components of a free-electron laser are an accelerator generating a bright, high-energy electron beam and a so-called undulator magnet. In the undulator, the electrons are forced on an oscillatory path by a periodic sequence of alternating transverse magnetic fields, and they emit radiation into a narrow bandwidth around a resonance wavelength λ_{ph} given by

$$\lambda_{ph} = \frac{\lambda_u}{2\gamma^2}\left(1+\frac{K^2}{2}\right), \text{ with } \gamma = \frac{E}{m_e c^2} \text{ and } K = \frac{eB_u\lambda_u}{2\pi m_e c}. \qquad (1)$$

Here, E is the electron energy, m_e the electron rest mass, e the elementary charge, c the speed of light in vacuum, λ_u the undulator period, and B_u is the peak magnetic field in the undulator.

While undulator radiation is widely used in synchrotron radiation sources to generate high-brilliance (photon flux per frequency bandwidth per unit phase space volume) ultraviolet and X-ray beams, a boost in intensity by many orders of magnitude is achieved in an FEL due to the interaction of the electrons with the radiation field generated in the undulator. If the charge density of the electron beam is sufficiently high and the undulator long enough, this interaction induces a periodic charge density modulation in the electron bunches with the period given by the resonance wavelength λ_{ph}. Once this so-called "microbunching" has been induced, many of the electrons start to radiate coherently at the resonant wavelength, thus increasing the radiation intensity and, in turn, the density modulation depth. This mechanism leads to an exponential growth of the radiation intensity along the undulator. The high-gain FEL[5-10] described here achieves laser amplification and saturation within a single pass of the electron bunch through the undulator and does not require a set of mirrors as is the case in conventional lasers and in the low-gain FEL. Thus, the high-gain FEL is suited for

wavelengths far below the visible where suitable mirrors are not available. The lasing process can be initiated by the spontaneous undulator radiation, and the FEL works then in the so-called Self-Amplified Spontaneous Emission (SASE) mode[5-10] without needing an external input signal.

Compared to storage-ring based synchrotron radiation sources[4], SASE FELs are capable of providing typically eight orders of magnitude higher peak brilliance with pulse lengths of about 100 fs FWHM and almost full transverse coherence. Two main advantages of the SASE FEL are revealed by Eq. (1): the tunability of the wavelength by varying the electron energy or the magnetic field and the possibility to achieve very short photon wavelengths at high electron energies. The shortest wavelength achieved with this principle up to now was 80 nm[11,12], which was promptly used for successful user-experiments[13,14].

2   The VUV-FEL at DESY

2.1 Overview

The experiments presented here have been performed at the Vacuum-Ultra-Violet Free-Electron Laser (VUV-FEL) at DESY, Hamburg[15]. A schematic layout is shown in Figure 1. The electron bunches are produced in a laser-driven photoinjector[16-18] and accelerated to 445 MeV by a superconducting linear accelerator[19]. Bunch charges between 0.5 and 1 nC are used. At intermediate energies of 125 and 380 MeV the electron bunches are longitudinally compressed[20,21], thereby increasing the peak current from initially 50–80 A to approximately 1–2 kA as required for the FEL operation. The 30 m long undulator[22] consists of NdFeB permanent magnets with a fixed gap of 12 mm, a period length of $\lambda_u = 27.3$ mm and peak magnetic field $B_u = 0.47$ T. Finally, a dipole magnet deflects the electron beam into a dump, while the FEL radiation propagates to the experimental hall.

2.2 Formation of electron beam

The FEL process demands a bunched electron beam of extremely high quality which can be produced by linear but not circular accelerators: specifically, high peak current, small emittance, small momentum spread and short bunch length. The injector consists of a laser-driven photocathode in a 1½ -cell radio-frequency (rf) cavity operating at 1.3 GHz with a peak accelerating field of 40 MV/m on the cathode[16,17]. The Cs$_2$Te cathode is illuminated by a Gaussian shaped UV laser pulse with 4 ps rms duration, generated in a mode-locked solid-state laser system synchronized with the rf. Since the bunch length extends over a non-negligible fraction of the rf wavelength of 23 cm, the particles in the bunch acquire a position-dependent momentum variation during the acceleration. This energy-position correlation is utilized to reduce the bunch length in two "bunch compressors", consisting of two magnetic chicanes. Here, the electrons with a larger momentum travel a shorter distance than those with smaller momentum thus enabling the bunch tail to catch up with the head if the appropriate longitudinal momentum profile has been imparted to the bunch. The expected longitudinal electron distribution within the bunch consists of a 50 fs long leading spike containing some 10% of the total charge with a peak current exceeding 1 kA, and a long tail with current too small from which to expect significant FEL gain. Since the particle distribution inside the bunch is longitudinally inhomogeneous, it is to be expected that each longitudinal slice of electrons inside the bunch acquires different values of the "slice" emittance and "slice" energy spread. Figure 2 illustrates the computed longitudinal structure of the bunches at the entrance of the undulator. The local particle energy E as well as the current I, the transverse ("slice") emittances $\varepsilon_{n,x}$ and $\varepsilon_{n,y}$ (normalized, see below), and the energy spread σ_E are plotted as a function of the internal time variable t.

The evolution of the electron beam in the accelerator depends on the accelerating electric fields and the magnetic guide fields, both acting on each electron independently,

and on collective forces such as space charge fields, transient wake fields generated by mirror charges in the metallic vacuum chamber and coherent synchrotron radiation. The essential goal of the FEL accelerator system is to produce beam of high peak current, small transverse emittance resulting in small beam size and small beam divergence, small momentum spread, and short bunch length. Rapid acceleration of the electrons to relativistic energies is essential to minimize the emittance increase by repulsive space charge forces inside the bunch. The emittance ε is, broadly speaking, the product of beam size and beam divergence. The "normalized emittance" $\varepsilon_n = \gamma\beta\varepsilon$ (with $\beta = v/c$, v being the speed of electrons, and $\gamma = (1 - \beta^2)^{-\frac{1}{2}}$), is a conserved quantity in a linear accelerator, if perturbing effects are avoided. Also, any energy chirp along the bunch should be small in order to prevent degradation of the FEL gain and an increase of the width of the photon spectrum. The parameter settings meeting the FEL requirements[21,23] were found with a number of numerical beam dynamics simulation tools[24,25]. For the bunch slice with maximum current (2 kA according to simulation of a 1 nC total charge) the normalized emittance is predicted to be $\varepsilon_n = 4\ \pi$ mm-mrad and the energy spread 300 keV, see Figure 2.

2.3 Superconducting accelerator

The electron injector section is followed by a total of five 12.2 m long accelerating modules each containing eight 9-cell superconducting niobium cavities, which provide the beam energy of 440 MeV required for 32 nm radiation wavelength according to Eq. (1). In the first three modules the electrons are accelerated on the slope of the rf wave to induce the position-dependent energy distribution within the bunch that is used for the longitudinal bunch compression. One "bunch compressor" is installed after the first accelerator module and a second one after the third accelerator module. In this way, emittance degradation due to coherent synchrotron radiation occurring in the bunch compressor dipole magnets can be minimized. The accelerator is actually capable of achieving much higher beam energy such that, in a next step of the

project, wavelengths around 10 nm are planned.

2.4 Electron beam diagnostics

The transverse electron beam size can be imaged using cameras observing the optical transition radiation generated when the electrons pass a thin, aluminium coated silicon wafer. From the data obtained at three locations with well-known beam-optical elements in between, the transverse beam emittance can be determined. We use four screens to improve the precision of the result and the quality of error analysis. The optical measurements are complemented by wire scanners. At 125 MeV, the measured emittance for 1 nC bunch charge is $\varepsilon_n = (2.0 \pm 0.4)$ mm-mrad (rms) without longitudinal bunch compression, in agreement with a numerical beam dynamics simulation done for the "no compression" case. It is noted that this method determines the emittance of the entire bunch, projected along the longitudinal axis, while the slice emittance of the compressed bunch (see Fig.2) is the important parameter for the FEL process. The measurement is nevertheless of quite some relevance since it indicates that the beam formation process is well understood.

The longitudinal beam profile has been determined using a streak camera, by electro-optical sampling[26] and by observation of the infrared coherent synchrotron radiation spectrum generated in the dipole magnets of the bunch compressors. A fourth method is based on the time-dependent deflection of the electron bunch induced by a rapidly rising electric field oriented perpendicular to the direction of beam motion[27,28]. This field is generated by a 2.8 GHz transverse mode cavity deflecting in the vertical direction. Analysis of the image observed on a downstream screen (see Figure 3) results in an upper limit of 120 fs FWHM for the length of the leading spike inside the electron bunch. By varying the strength of a quadrupole magnet located upstream of this device, it is also possible to determine the slice emittance. One might argue that this can only work in the direction perpendicular to the deflecting field, i.e. in the horizontal plane.

However, in a case like ours with an isolated steep spike, also the vertical emittance of the spike can be extracted from the variation of its vertical size on the screen when scanning the quadrupole strength. First measurements of the compressed bunch result in a horizontal emittance of the lasing spike of $\varepsilon_{x,n} = (2.9 \pm 0.3)\,\pi\,\mathrm{mm} \cdot \mathrm{mrad}$ and a vertical emittance of $\varepsilon_{y,n} = (4.3 \pm 0.4)\,\pi\,\mathrm{mm} \cdot \mathrm{mrad}$, in reasonable agreement with expectations shown in Fig. 2.

2.5 Undulator

The undulator[22] system is subdivided into six segments, each 4.5 m long. In a 60 cm long space between the segments, quadrupole magnets to focus the electron beam and electron beam diagnostics tools, such as wire scanners and beam position monitors, are installed. Achieving a perfect overlap of the electron beam with the radiation field generated inside the undulator is mandatory for the FEL process. Therefore, the utmost care is taken in aligning all the elements. A very high field quality has been achieved in the undulator modules so that the expected rms deviations of the electrons from the ideal orbit should be less than 10 μm.

3 FEL radiation properties

The properties of FEL radiation[21] have been calculated for 30 nm wavelength with the three-dimensional, time-dependent simulation code FAST[29], predicting an average energy in the radiation pulse of up to 100 μJ for a bunch charge of 1 nC.

The most critical step has been to find the onset of laser amplification. For this purpose a radiation detector equipped with a microchannel plate (MCP) has been used, which features a dynamical range of seven orders of magnitude and covers the entire range of intensities from spontaneous emission up to FEL saturation[30]. The MCP measures the radiation scattered by a gold mesh placed behind a 10 mm aperture located 18.5 m downstream of the undulator. Behind this aperture, the background signal from

spontaneous undulator-radiation is approximately 7 nJ for a bunch charge of 1 nC. The 1% relative measurement accuracy of the MCP is sufficient for a reliable detection of the onset of FEL gain above the spontaneous background. The VUV-FEL has been tuned to an average energy of 10 µJ in the radiation pulse, corresponding to $1.6 \cdot 10^{12}$ photons. So far, pulse energies of up to 40 µJ have been observed. At high pulse energies (>0.5 µJ) the MCP detector was cross-calibrated with a relative uncertainty of ±25% against a gas monitor detector used as a transfer standard[31]. Keeping in mind that only a small coherent fraction of the spontaneous undulator-radiation is amplified, an FEL gain of about 10^6 can be deduced from these data.

Figure 4 shows the image of a single VUV-FEL pulse on a Ce:YAG crystal mounted behind the gold mesh of the MCP detector. The wires are clearly visible. From the wire spacing of 0.31 mm, image analysis yields a spot size of 3 mm FWHM. This corresponds to an angular divergence of (130 ± 30) µrad FWHM, the error being mainly due to the uncertainty in the longitudinal origin of the FEL radiation. There is good agreement with the simulated angular divergence of 140 µrad in the far zone (right hand side of Figure 4). We conclude that the observed angular divergence is close to the diffraction limit which is a clear indication for a high degree of transverse coherence.

Figure 5 shows the measured energies of many successive radiation pulses. A large fluctuation is seen which is to be expected since in a SASE FEL the gain process starts from shot noise. Theoretically, the radiation pulse energy should fluctuate according to a Gamma distribution

$$p(E) = \frac{M^M}{\Gamma(M)} \left(\frac{E}{\langle E \rangle} \right)^{M-1} \frac{1}{\langle E \rangle} \exp\left(-M \frac{E}{\langle E \rangle} \right) \quad \text{with} \quad M = \frac{\langle E \rangle^2}{\left\langle \left(E - \langle E \rangle \right)^2 \right\rangle} \qquad (2)$$

provided the FEL gain process is in the regime of exponential growth[10,32]. Here <E> is the mean photon pulse energy, and Γ is the gamma function. The parameter *M* is the inverse of the normalized variance of *E*. It defines the number of optical modes in the

radiation pulse and provides a relationship between the average number of spikes in the single-pulse wavelength spectra and the fluctuations of pulse energy. The measured histogram in the lower part of Figure 5 fits nicely the Gamma distribution Eq. (2) with $M = 4.1$. The statistical analysis cannot distinguish between transverse and longitudinal modes. Since a high degree of transverse coherence has already been concluded from the observed angular divergence, the transverse mode number should be less than two. Consequently, we expect three to four longitudinal modes. According to statistical analysis and numerical simulation, this implies that, on average, two wave packages ("spikes") should be present in the time profile of each FEL radiation pulse.

While the ultra-short pulse duration has up to now precluded a direct measurement of the temporal structure of the FEL pulses, the single-pulse wavelength spectra are accessible and may be used to estimate the radiation pulse duration. Three such spectra are presented in Figure 6. They were taken with a grating spectrometer (0.04 nm resolution) equipped with an intensified CCD camera[33]. The FWHM pulse duration is obtained from the typical width $\Delta\omega$ of the spikes in the single-pulse spectra using the relation $\tau_{rad} \cong 2\pi/(\Delta\omega) \cong (25 \pm 5)$ fs. With the average radiation pulse energy of 10 μJ, this corresponds to an average power of 0.4 GW within the FEL pulse and approx. 1 GW inside the spikes. The average number of such spikes within the bandwidth of the FEL (given by the wavelength spectrum averaged over many FEL pulses) scales with the number of longitudinal modes. This number is about two, in agreement with our expectation from the fluctuation analysis. As shown in the lower part of Figure 6, there is again good agreement with both the predicted FEL bandwidth and the width of the spikes. Note that the radiation pulse length estimated here from the analysis of spike widths agrees well with the numerical simulations based on a 50 fs long leading spike in the electron bunch profile mentioned before.

We note that the FWHM pulse duration of radiation pulses at the VUV-FEL has been determined at $\tau_{rad} = (25 \pm 5)$ fs in three entirely independent ways:

1. Spectral analysis of the spiky structure of single-pulse wavelength spectra, see Figure 6.

2. Statistical analysis of pulse-to-pulse intensity fluctuations, see Figure 5.

3. Time-domain measurement of the longitudinal electron bunch profile (see Figure 3) corroborates the existing of such a short, leading spike. It is in qualitative agreement with the result from numerical beam dynamics simulation and subsequent numerical simulation of the FEL process.

A figure of merit relevant for many experiments is the brilliance. For transversely coherent radiation sources, it is defined as $brilliance = \dfrac{spectral\ flux}{(\lambda/2)^2}$. For the VUV-FEL photon beam described here, the peak brilliance is in the order of 10^{28} photons/$(s \cdot mm^2 \cdot mrad^2 \cdot 0.1\%\ bandwidth)$, about seven orders of magnitude above the state-of-the-art of synchrotron radiation sources.

4 Conclusion

In conclusion, we have demonstrated during the first operation of the VUV-FEL at DESY that powerful, laser-like VUV radiation pulses in the 10 fs range can be produced with a simple and reliable single-pass SASE FEL scheme.

Acknowledgements

References

1. *A VUV Free Electron Laser at the TESLA Test Facility at DESY. Conceptual Design Report*, DESY, TESLA-FEL **95-03** (1995).

2. F. Richard *et al*., (Eds.), TESLA Technical Design Report, *DESY* **2001-11** (2001) and `http://tesla.desy.de` .

3. The LCLS Design Study Group: LCLS Design Study Report, SLAC-R521, Stanford (1998) and `http://www-ssrl.slac.stanford.edu/lcls/CDR` .

4. R. Brinkmann *et al*., (Eds..), TESLA XFEL: First stage of the X-ray laser laboratory-Technical design report, *DESY* **2002-167** (2002) and `http://xfel.desy.de` .

5. A.M. Kondratenko, E.L. Saldin, Generation of Coherent Radiation by a Relativistic Electron Beam in an Undulator, Part. Accelerators **10,** 207 (1980).

6. Ya.S. Derbenev, A.M. Kondratenko, E.L. Saldin, On the possibility of using a free electron laser for polarization of electrons in storage rings, Nucl. Instrum. and Methods **193,** 415 (1982).

7. R. Bonifacio, C. Pellegrini, L.M. Narducci, Collective instablities and high-gain regime in a free electron laser, Optics Commun. **50 ,** 373 (1984).

8. K.J. Kim, Three-dimensional analysis of coherent amplification and self-amplified spontaneous emission in free-electron lasers, Phys. Rev. Lett. **57** , 1871 (1986).

9. S. Krinsky, L.H. Yu, Output power in guided modes for amplified spontaneous emission in a single-pass free-electron laser, Phys. Rev. **A35,** 3406 (1987).

10. E.L. Saldin, E.A. Schneidmiller, M.V. Yurkov, *The Physics of Free Electron Lasers,* (Springer, Berlin, 1999).

11. V. Ayvazyan *et al*., Generation of GW radiation pulses from a VUV free-electron laser operating in the femtosecond regime, Phys. Rev. Lett. **88,** 104802 (2002).

12. V. Ayvazyan *et al*., A new powerful source for coherent VUV radiation: Demonstration of exponential growth and saturation at the TTF free-electron laser, Eur. Phys. J. **D20**, 149 (2002).

13. H. Wabnitz *et al.,* Multiple ionization of atom clusters by intense soft X-rays from a free electron laser, Nature **420,** 482 (2002).

14. L. Juha *et al*., Ablation of various materials with intense XUV radiation, Nucl. Instrum. and Methods **A 507**, 577 (2003).

15. The TTF FEL team, SASE FEL at the TESLA Test Facility, Phase 2, DESY Print TESLA-FEL **2002-01** (2002).

16. M. Krasilnikov *et al.*, Optimizing the PITZ Electron Source for the VUV FEL, *Proc. EPAC 2004 Conference*, Lucerne, Switzerland, 360 (2004).

17. S. Schreiber, Commissioning of the VUV-FEL Injector at TTF, *Proc. EPAC 2004 Conference*, Lucerne, Switzerland, 351 (2004).

18. K. Flöttmann, Ph. Piot, An Upgraded Injector for the TTF FEL User Facility, *Proc. EPAC 2002 Conference*, Paris, France, 1798 (2002).

19. H. Weise, Superconducting RF Structures - Test Facilites and Results, *Proc. 2003 Part. Acc. Conf.,* Portland, Oregon, 673 (2003).

20. T. Limberg *et al.*, Design and Performance Simulation of the TTF-FEL II Bunch Compression System, *Proc. EPAC 2002 Conference,* Paris, France, 811 (2002).

21. E.L. Saldin, E.A. Schneidmiller, M.V. Yurkov, Expected properties of the radiation from VUV-FEL at DESY (femtosecond mode of operation), DESY Print TESLA-FEL **2004-06** (2004).

22. J. Pflüger, Undulators for SASE FELs, Nucl. Instrum. and Methods **A445,** 366 (2000).

23. M. Dohlus *et al*., Start-to-end simulations of the SASE FEL at the TESLA Test Facility, phase 1, Nucl. Instrum and Methods **A 530,** 217 (2004).

24. K. Flöttmann, Astra User Manual, `http://www.desy.de/~mpyflo/Astra_dokumentation/` .

25. M. Borland, `elegant`: A flexible SDDS-Compilant Code for Accelerator Simulation, APS LS-**287** (September 2000).

26. B. Steffen et al., EOS Electro Optical Bunch Length Measurements at the VUV-FEL at DESY, *Proc. 2005 Part. Acc. Conf.,* Knoxville, TN, USA (2005).

27. P. Krejcik *et al.*, Commissioning of the SPPS Linac Bunch Compressor, *Proc. 2003 Part. Acc. Conf*., Portland, Oregon, 423 (2003).

28. R. Akre *et al*., Bunch length measurements using a transverse RF deflecting structure in the SLAC linac, *Proc. EPAC 2002 Conference,* Paris, France (2002).

29. E.L. Saldin, E.A. Schneidmiller, M.V. Yurkov, FAST: a three-dimensional time-dependent FEL simulation code, Nucl. Instrum. and Methods **A429**, 233 (1999).

30. A. Bytchkov *et al*., Development of MCP-based photon diagnostics a the TESLA Test Facility at DESY, Nucl. Instrum. and Methods **A528**, 254 (2004).

31. M. Richter *et al*., Measurement of Gigawatt radiation pulses from a vacuum and extreme ultraviolet free-electron laser, Appl. Phys. Lett., **83**, 2970 (2003).

32. E.L. Saldin, E.A. Schneidmiller, M.V. Yurkov, Statistical properties of radiation from VUV and X-ray free electron lasers, Opt. Commun. **148**, 383 (1998).

33. P. Nicolosi *et al*., On-line spectral monitoring of the VUV-FEL beam at DESY, *Proc. 2004 FEL Conference,* Trieste, Italy, 415-128 (2004).
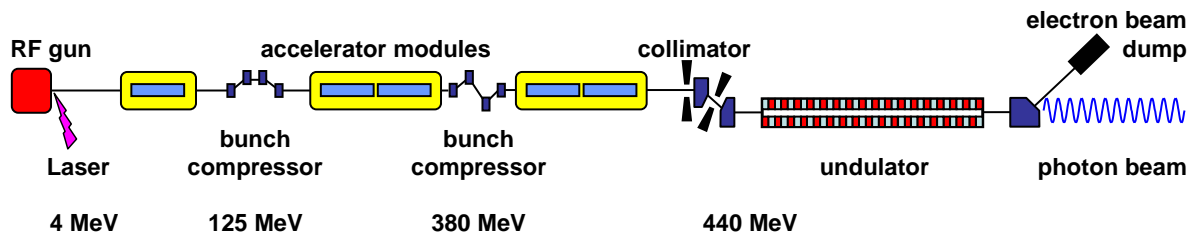
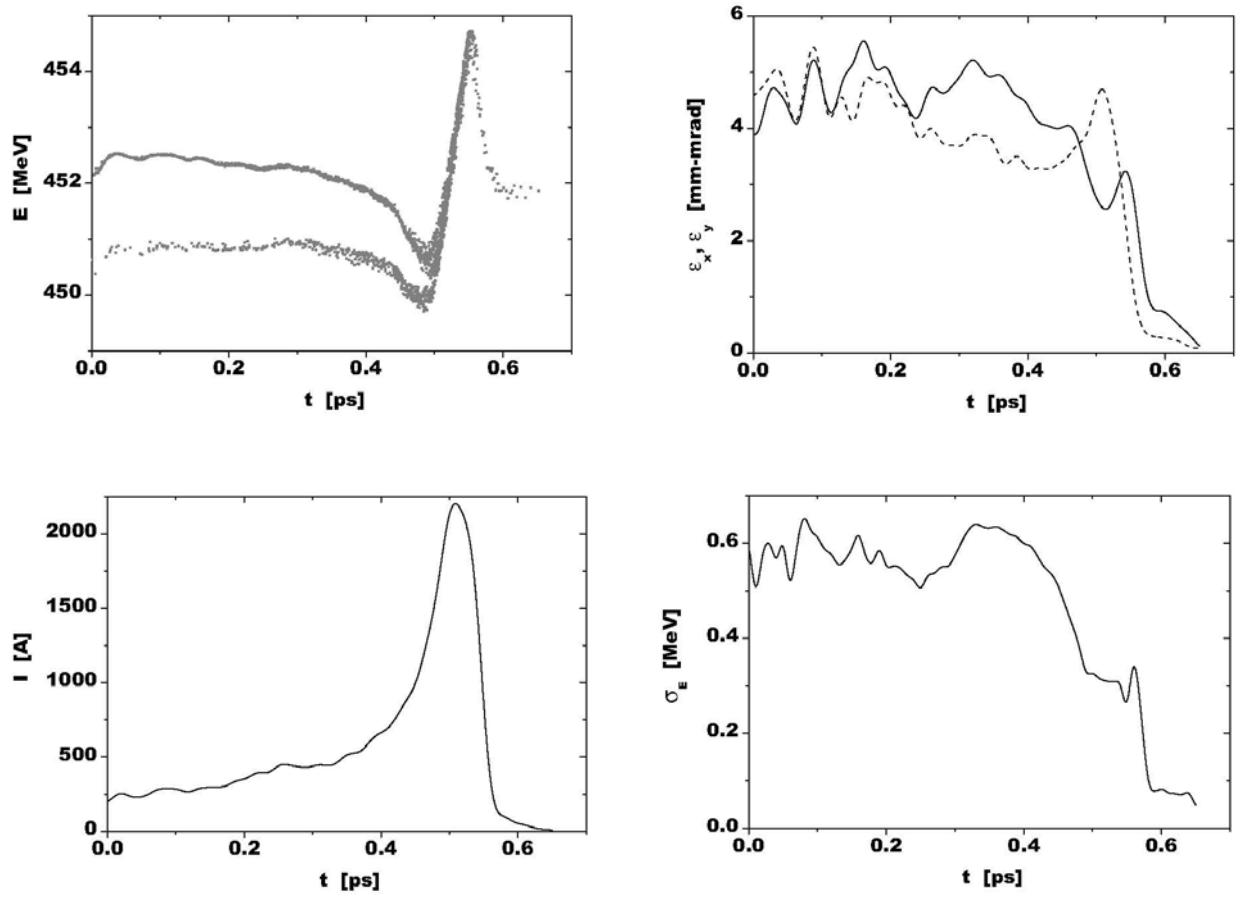Figure 1: Schematic layout of the VUV-FEL at DESY, Hamburg.

Figure 2: Longitudinal structure of a 1 nC electron bunch at the entrance of the undulator according to numerical beam dynamics simulation[21]. Top left: Local particle energy E. In the tail of the bunch, the energy distribution is broken in two branches. Bottom left: Current I. Top right: Normalized, transverse ("slice") emittances ε_x (solid line) and ε_y (broken line). Bottom right: rms energy spread σ_E. All parameters are plotted as a function of the internal time variable t. The bunch head is to the right hand side.
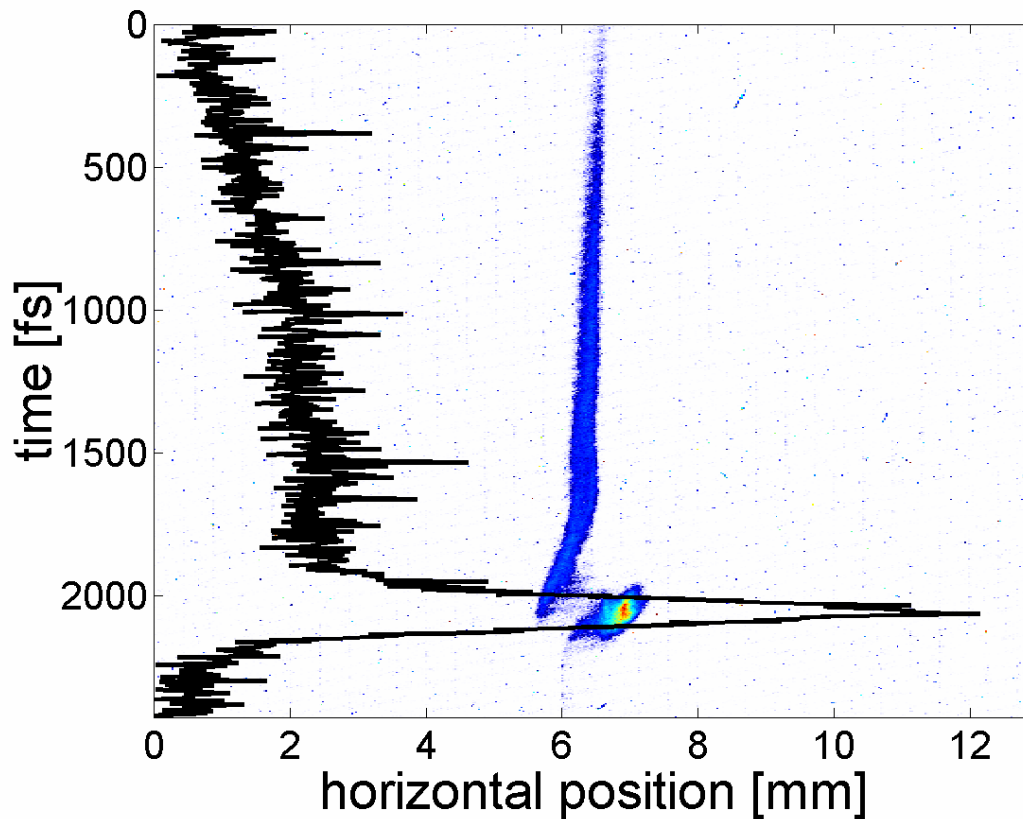
Figure 3: Charge distribution within a single electron bunch of the VUV-FEL at DESY. In the centre, the image of the bunch on an observation screen is seen, located downstream of a transverse mode cavity resonator streaking the bunch vertically by a time dependent electric field. The horizontal position of electrons is given on the horizontal axis, while the relative longitudinal position inside the bunch is encoded in the vertical coordinate, given in fs units, with the head of the bunch to the bottom. The solid curve shows the charge density projected onto the longitudinal position, i.e. the electric current profile within the bunch. A sharp spike shorter than 120 fs (FWHM) is seen at the head of the bunch.
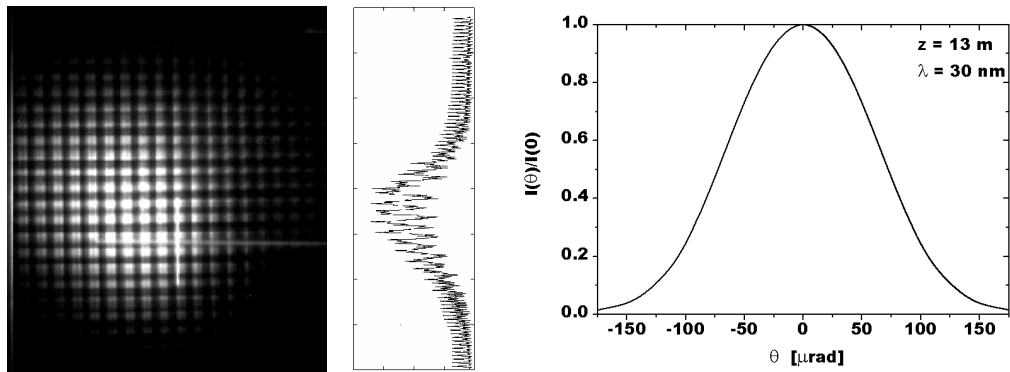
Figure 4: Left: Image of a single radiation pulse of the VUV-FEL on a CeYaG crystal behind the gold wire mesh of the MCP detector, located 18.5 m downstream of the undulator. The distance between wires is 0.31 mm. Right: Simulated angular distribution of the radiation intensity in the far zone[21].
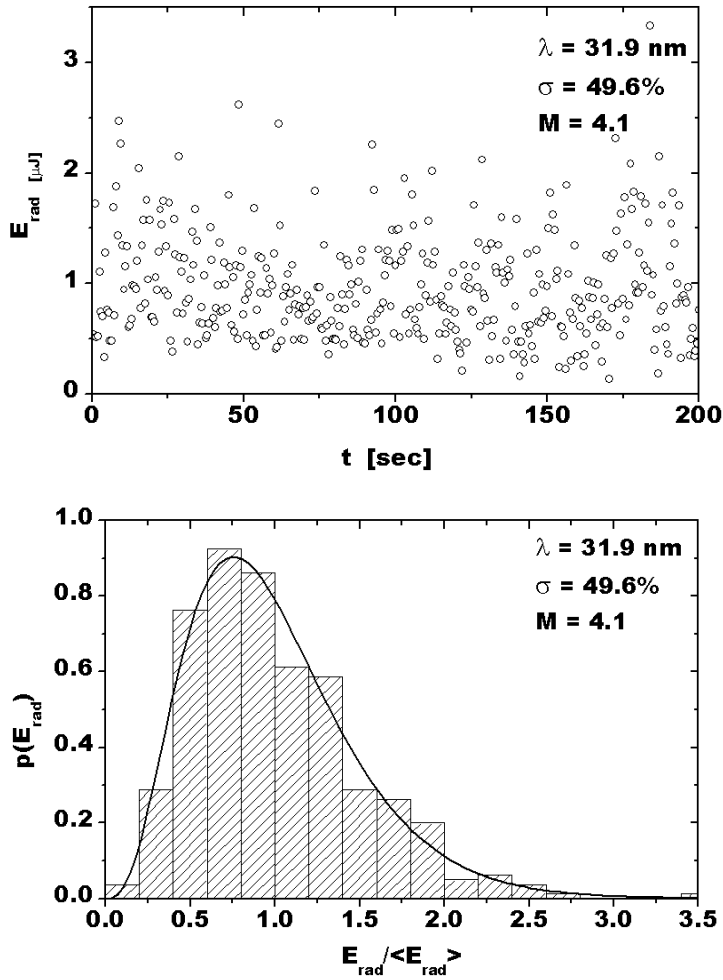
Figure 5: Measured FEL-pulse energies for many successive pulses. Top: pulse to pulse variation of FEL energy. Bottom: Measured probability distribution of the radiation energy (histogram). The solid curve represents the Gamma distribution $p(E,)$ of Eq. (2) for M=4.1 which is calculated from the variance of pulse energy fluctuations illustrated in the upper part of the figure. This is the expected distribution of a high-gain FEL operating in the exponential regime. The measurement confirms that the VUV-FEL is operating in the exponential regime and is a source of completely chaotic polarized radiation[10,32], with M being the total number of optical modes in the pulse.
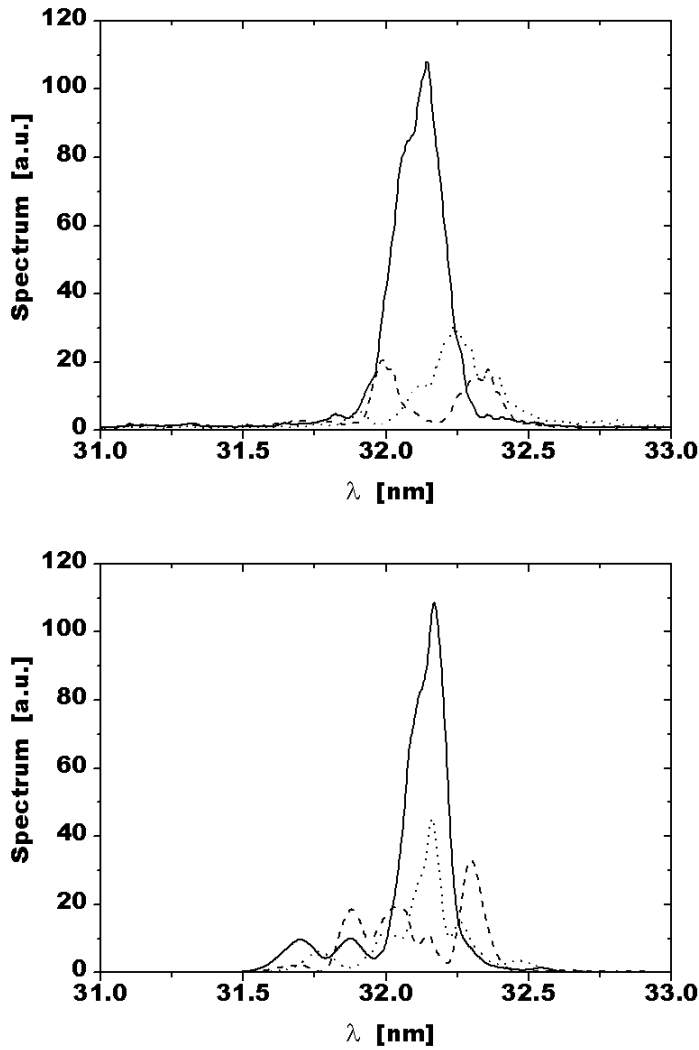
Figure 6: Top: Three single-shot wavelength spectra of FEL radiation pulses measured at the VUV-FEL. Bottom: Simulation of the spectral structure of the VUV-FEL operating in the exponential regime[21]. Three different shots are shown with different line shapes (solid, dashed, and dotted). Note that the number of spikes in the spectrum is in average equal to the number of spikes (coherent wave packets) in the time domain.